

Phonon-assisted decoherence in coupled quantum dots

A. Thilagam and M. A. Lohe

*Department of Physics,
The University of Adelaide, Australia 5005*

(Dated: September 22, 2018)

We analyse various phonon-assisted mechanisms which contribute to the decoherence of excitonic qubits in quantum dot systems coupled by the Förster-type transfer process. We show the significant loss of coherence accompanied by dissipation due to charge carrier oscillations between qubit states by using a model of one-phonon assisted Förster-type transfer process. We obtain explicit expressions for the relaxation and dephasing times for excitonic qubits interacting with acoustic phonons via both deformation potential and piezoelectric coupling. We compare the decoherence times of the GaAs/AlGaAs material system with half times of concurrence decay in a $2 \otimes 2$ bipartite mixed excitonic qubit system. We extend calculations to determine the influence of phonon mediated interactions on the non-unitary evolution of Berry phase in quantum dot systems.

PACS numbers: 03.67.Lx, 03.67-a, 78.67.Hc, 73.20.Mf, 85.35.Gv

I. INTRODUCTION

The use of excitons (electron-hole correlated states) in quantum dots has generated great interest as suitable devices for the solid-state implementation of quantum logic gates^{1,2,3,4}. The significant advancement in creating and probing excitonic states in quantum dots^{5,6} and newly developed techniques which allow quantum coupling between excitonic states to be continuously varied by external electric fields⁴ has provided rapid progress in the field of solid-state quantum computation. In the case of two coupled quantum dot systems, exciton-exciton dipole interactions give rise to diagonal terms which allows quantum logic to be performed via ultra-fast laser pulses on time scales less than calculated decoherence times². Related studies^{7,8,9} have suggested the importance of the Förster energy transfer process in producing entangled excitonic states and using external electric fields to achieve critical logic gate actions. Dipole-dipole interaction was first proposed by Förster¹⁰ and further extended by Dexter¹¹ as a mechanism of energy transfer in which excitonic wavefunctions localized at different quantum dots do not overlap.

Other than the actual generation of entangled excitonic qubit states, the successful implementation of quantum logic systems depends critically on the decoherence properties of the qubits. Decoherence due to environmental factors such as phonons and impurities is inevitable and is regarded as a major drawback in solid-state devices. Several strategies such as decoherence-free subspaces^{12,13}, optimal control techniques¹⁴ and immunization processes¹⁵ have been proposed to counter the detrimental effects of decoherence. Geometric quantum computation has gained increased status as a robust fault-tolerant scheme in recent years^{16,17}. The geometric phase component (Berry phase) of the phase shift in quantum states relies solely on the global geometry of the path executed during cyclical evolution and hence is manifestly gauge invariant and consequently insensitive to stochastic operation errors¹⁸. It is not immediately clear however whether these proposals invoke other routes which facilitate decoherence and if so the role played by various system parameters in minimizing errors during logic gate operations. Hence there is a need to scrutinize the various intrinsic processes and in particular phonon induced types in order to achieve fault tolerant quantum switches.

The interaction of charge carriers with acoustic phonons arises mainly from deformation-potential and piezoelectric coupling in quantum dots¹⁹. Theoretical estimates by Fedichkin *et al*²⁰ show that the error rate due to acoustic phonons may be a major factor limiting qubit performance, in agreement with experimental results²¹ of a qubit system implemented using a double-dot GaAs/AlGaAs system with a two dimensional electron gas. Electron-phonon interaction has been shown to be significant in GaAs/InAs quantum dots compared to the bulk system of the same material leading to the formation of polarons²². In another work, Jacak and coworkers have studied the significance of relaxation of electrons surrounded by a cloud of phonons due to the anharmonic interaction of optical phonons with acoustic phonons in GaAs/InAs quantum dot systems²³. A recent study²⁴ has considered the possibility of localization²⁵ in which an electron state delocalized over two quantum dots is converted into a mixture of two classical-like localized states and consequently loses its coherence to the surrounding reservoir of phonons.

The interaction of qubits with phonons is generally modelled as a first-order process taking into account only the coupling of carrier states localized in quantum dots²⁶ in contact with a phonon bath. The interaction of charge carriers with phonons as the qubit flips back and forth between the quantum dots has not been well investigated in earlier studies related to phonon mediated decoherence in semiconductor systems^{20,27,28}. The loss of coherence due to charge carrier movements during oscillations between the different qubit states is unavoidable, and therefore we aim to closely examine this critical mode of decoherence in this work. We model this route of degradation in the purity and entanglement of qubit states to proceed via a one-phonon assisted oscillation of qubit states leading to

relaxation as well as dephasing of the qubit states. In order to obtain explicit results, we consider the specific case of excitonic qubits in Förster coupled quantum dots⁸. An earlier work⁹ has examined the coupling of the Förster coupled quantum dot system to the external environment consisting of a single radiation mode and the associated spontaneous emission and decay processes. We are unaware of other detailed studies of phonon mediated interactions involving excitonic qubit states in Förster coupled quantum dots.

It is not immediately clear whether decoherence phenomenon is dominated by relaxation or pure dephasing process and the extent to which the outcome is affected by the nature of qubit-phonon coupling during a cycle of logic gate operation. The subtle difference between relaxation and pure dephasing of entangled systems has to be emphasized. While relaxation brings about shifts in the population of qubits states with one state favored over another, pure dephasing process results in changes in the energy difference between qubit states with the population of qubit states remaining intact. While both processes lead to decoherence of the entangled system, we aim to examine the various parameters affecting the two inherent sources of dissipation in this work. Our approach undertaken here can be extended to other designs of coupled dot qubit systems such as the electrically controlled charge qubit in the double quantum dot system or the double impurity semiconductor systems²⁹.

It is well known that a quantum system exposed to an environment is best described by the reduced density matrix for which approximation techniques³⁰ have been developed to describe the quantum state evolution at times determined by the environmental noise. Non-Markovian stochastic Schrodinger equations³¹, Lindblad³² and Redfield master equations³³ have been independently used to investigate the dynamics of open quantum system in contact with noisy environments. In a recent work, Braun³⁴ showed that two qubits not interacting directly but which are in contact with a common environment can become entangled and the entanglement may last for a long time depending the strength of coupling and environmental conditions. These results are similar to those obtained by Ficek et al³⁵ who studied a system of two suitably prepared atoms immersed in a vacuum field. The term "sudden death" has been coined in an earlier work³⁶ to describe the process in which two initially entangled atoms which become noninteracting later become completely disentangled in relatively short times. The presence of such features have not been thoroughly investigated in excitonic qubit systems.

In the second part of this work, we investigate the dynamical behaviour of entanglement of excitons coupled to two phonon baths associated with deformation-potential and piezoelectric coupling in the absence of a direct channel of interaction, i.e the Förster interaction is switched off by control of external electric fields. We follow the approach of Tolkmunov et al³⁷ in which the degree of loss of coherence is determined by the decay of the off-diagonal terms of the reduced density matrix. We determine two important quantities, namely the Berry phase and concurrence³⁸ and show the strong correlation between the Berry phase correction fraction which quantify departure from unitary evolution and half times of concurrence decay in GaAs/AlGaAs quantum dots.

II. EXCITONIC QUBITS IN QUANTUM DOTS

We consider two excitons in their ground states in adjacent coupled quantum dots located at \mathbf{R}_a and \mathbf{R}_b . We assume the quantum dots to be shaped in the form of either cuboid boxes or quasi-two dimensional disks in which the vertical confinement energies of charge carriers are larger than their lateral confinement energies. We label the localized excitonic states as $|\mathbf{R}_a\rangle$ and $|\mathbf{R}_b\rangle$. Employing some of the notations in our earlier works³⁹, we represent $|\mathbf{R}_a\rangle$ as

$$|\mathbf{R}_a\rangle = \frac{\nu_0}{L} \sum_{\mathbf{r}_e, \mathbf{r}_h} \Phi(\mathbf{R}_a, \mathbf{r}_{e\parallel}, \mathbf{r}_{h\parallel}, z_e, z_h) a_{c, \mathbf{r}_e}^\dagger a_{v, \mathbf{r}_h} |\mathbf{0}\rangle, \quad (1)$$

where ν_0 is the volume of the unit cell, L is the quantization length and $a_{c, \mathbf{r}_e}^\dagger$ (a_{v, \mathbf{r}_h}) is the creation (annihilation) operator of an electron in the conduction (valence) band, denoted by c (v). $|\mathbf{0}\rangle$ in Eq. 1 denotes the electronic state of the quantum dot in which all electronic ground states are occupied and all excited states are unoccupied. For simplicity, we ignore the role of spin effects and spin indices in Eq. 1. The position vectors \mathbf{r}_e and \mathbf{r}_h are decomposed into components parallel and perpendicular to the lateral direction of the quantum dot as $\mathbf{r}_e = (\mathbf{r}_{e\parallel}, z_e)$ and $\mathbf{r}_h = (\mathbf{r}_{h\parallel}, z_h)$. The vertical confinement energies of charge carriers are stronger than the lateral confinement energies, the exciton wavefunction and therefore we factorise $\Phi(\mathbf{R}_a, \mathbf{r}_{e\parallel}, \mathbf{r}_{h\parallel}, z_e, z_h)$ as

$$\Phi(\mathbf{R}_a, \mathbf{r}_{e\parallel}, \mathbf{r}_{h\parallel}, z_e, z_h) = \Psi(\mathbf{R}_a, \mathbf{r}_{e\parallel}, \mathbf{r}_{h\parallel}) \varphi_e(z_e) \varphi_h(z_h), \quad (2)$$

where $\varphi_e(z_e)$ ($\varphi_h(z_h)$) is the envelope function of the electron (hole) in the vertical direction of the quantum dot. The form of the in-plane exciton wavefunction $\Psi(\mathbf{R}_a, \mathbf{r}_{e\parallel}, \mathbf{r}_{h\parallel})$ at \mathbf{R}_a depends on the degree of confinement of the electron-hole within the quantum dot. We consider a strong individual charge carrier regime in which the kinetic motions of the electron and holes are quantized separately so that the resulting discrete energy levels are affected

by the Coulomb interaction between the electron and hole only by a small amount of the order $\approx \frac{1}{L}$ where L is the quantum dot radius.

$\Psi(\mathbf{R}_a, \mathbf{r}_{e\parallel}, \mathbf{r}_{h\parallel})$ is further factorized using a suitable change of coordinates

$$\begin{aligned}\mathbf{r}_{\parallel} &= \frac{1}{l_r}(\mathbf{r}_{e\parallel} - \mathbf{r}_{h\parallel}) \\ \mathbf{R} &= \frac{1}{l_r^2}(l_h^2 \mathbf{r}_{e\parallel} - l_e^2 \mathbf{r}_{h\parallel})\end{aligned}$$

where $l_r = \sqrt{l_e^2 + l_h^2}$. The effective lengths l_e and l_h are related to the respective electron and hole effective masses and confining potential frequencies, ω_o^e and ω_o^h by $l_e = \sqrt{\frac{\hbar}{m_e \omega_o^e}}$ and $l_h = \sqrt{\frac{\hbar}{m_h \omega_o^h}}$. We obtain $\Psi(\mathbf{R}_a, \mathbf{r}_{e\parallel}, \mathbf{r}_{h\parallel}) = \Xi(\mathbf{R}, \mathbf{R}_a) \psi(\mathbf{r}_{\parallel})$ where the confining potential in the lateral direction are modelled using harmonic potentials

$$\begin{aligned}\psi(\mathbf{r}_{\parallel}) &= \frac{1}{\sqrt{\pi} l_r} \exp\left(-\frac{r_{\parallel}^2}{2l_r^2}\right), \\ \Xi(\mathbf{R}, \mathbf{R}_a) &= \frac{1}{\sqrt{\pi} L_R} \exp\left(-\frac{1}{2L_R^2} |\mathbf{R}_{\parallel} - \mathbf{R}_a|^2\right)\end{aligned}\quad (3)$$

where $L_R^2 = l_e^2 l_h^2 / l_r^2$. The length scales l_e and l_h associated with the harmonic potential are smaller than the effective Bohr radius of the exciton due to the strong confinement of charge carriers in the quantum dot.

The Gaussian form of function $\Xi(\mathbf{R}, \mathbf{R}_a)$ in Eq. 3 yields an explicit expression for its two-dimensional Fourier transform:

$$\begin{aligned}\Xi(\mathbf{R}, \mathbf{R}_a) &= \int d^2 \mathbf{q}_{\parallel} \exp(i \mathbf{q}_{\parallel} \cdot \mathbf{R}) \tilde{\Xi}(\mathbf{R}, \mathbf{R}_a), \\ \tilde{\Xi}(\mathbf{R}, \mathbf{R}_a) &= \frac{L_R}{2\pi \sqrt{\pi}} \exp(-i \mathbf{q}_{\parallel} \cdot \mathbf{R}_a - \frac{L_R^2 q_{\parallel}^2}{2})\end{aligned}\quad (4)$$

The confining potential in the vertical direction are modelled using harmonic potentials defined by the vertical confinement dimensions l_{ze} and l_{zh} respectively for electrons and holes

$$\begin{aligned}\varphi_e(z_e) &= \left(\frac{1}{\sqrt{\pi} l_{ze}}\right)^{\frac{1}{2}} \exp\left(-\frac{z_e^2}{2l_{ze}^2}\right), \\ \varphi_h(z_h) &= \left(\frac{1}{\sqrt{\pi} l_{zh}}\right)^{1/2} \exp\left(-\frac{z_h^2}{2l_{zh}^2}\right),\end{aligned}\quad (5)$$

The excitonic state $|\mathbf{R}_b\rangle$ is analogous in form to Eq. 1.

We code the excitonic qubits states using the relative position of the exciton via the basis set, $(|\mathbf{L}\rangle, |\mathbf{R}\rangle)$

$$\begin{aligned}|\mathbf{L}\rangle &= |\mathbf{R}_a\rangle \otimes |\mathbf{0}\rangle_b \\ |\mathbf{R}\rangle &= |\mathbf{0}\rangle_a \otimes |\mathbf{R}_b\rangle,\end{aligned}\quad (6)$$

The states, $|\mathbf{0}\rangle_a$ and $|\mathbf{0}\rangle_b$, which correspond to the absence of excitons denote the respective ground states of the quantum dots at $|\mathbf{R}_a\rangle$ and $|\mathbf{R}_b\rangle$. We simplify the approach by considering a two-level system involving only the states $|\mathbf{L}\rangle$ and $|\mathbf{R}\rangle$ and work in the limit of a pure Förster coupling. The direct Coulomb interaction which causes the formation of the biexciton state $|\mathbf{R}_a\rangle |\mathbf{R}_b\rangle$ is neglected. We also exclude the possibility of entangled states involving the vacuum state, $|\mathbf{0}\rangle_a |\mathbf{0}\rangle_b$. The two level excitonic qubit Hamiltonian is written as

$$\hat{H}_{\text{ex-qb}} = -\hbar \left(\frac{\Delta\Omega}{2} \sigma_z + F \sigma_x \right), \quad (7)$$

where the Pauli matrices $\sigma_z = |\mathbf{L}\rangle \langle \mathbf{R}| + |\mathbf{R}\rangle \langle \mathbf{L}|$ and $\sigma_x = |\mathbf{L}\rangle \langle \mathbf{L}| - |\mathbf{R}\rangle \langle \mathbf{R}|$. $\Delta\Omega = \Omega_a - \Omega_b$ is the difference in exciton creation energy between the quantum dot at \mathbf{R}_a and that at \mathbf{R}_b . F denotes the interdot Förster interaction amplitude responsible for the transfer of an exciton from one quantum dot to the other without involving a tunnelling process.

The eigenstates of the interacting qubit system in Eq. 7 appear as

$$\begin{aligned}|\chi_s\rangle &= \cos(\beta/2) |\mathbf{L}\rangle + \sin(\beta/2) |\mathbf{R}\rangle \\ |\chi_{as}\rangle &= \sin(\beta/2) |\mathbf{L}\rangle - \cos(\beta/2) |\mathbf{R}\rangle,\end{aligned}\quad (8)$$

with eigenenergies

$$\begin{aligned} E_{\text{as}} &= \Omega_0 + \Omega_1 - \frac{\Delta\Omega}{2} - \sqrt{\left(\frac{\Delta\Omega}{2}\right)^2 + F^2}, \\ E_{\text{s}} &= \Omega_0 + \Omega_1 - \frac{\Delta\Omega}{2} + \sqrt{\left(\frac{\Delta\Omega}{2}\right)^2 + F^2}, \end{aligned} \quad (9)$$

Ω_0 denotes the ground state energy of the system in which both the quantum dots are not occupied by excitons while Ω_1 denotes a higher energy level of the excitonic qubit system. The energy difference between the eigenstates is $\sqrt{\Delta\Omega^2 + (2F)^2}$ and can be studied as a function of time. In the absence of any decoherence process, the excitonic qubit oscillates coherently between the two dots with the Rabi frequency $E_{\text{s}} - E_{\text{as}}$. The polar angle β in the Bloch sphere representation of a qubit is related to $\Delta\Omega$ and F via

$$\tan \beta = \frac{2F}{\Delta\Omega} \quad (10)$$

III. INTERDOT FÖRSTER AMPLITUDE TERM F

The magnitude of the interdot Förster amplitude F is given by the matrix element

$$\begin{aligned} F &= \langle \mathbf{R} | \hat{H}_F | \mathbf{L} \rangle \\ &= \sum_{\mathbf{r}_a, \mathbf{r}_b} \langle g, \mathbf{R}_a; f, \mathbf{R}_b | U(|\mathbf{r}_a - \mathbf{r}_b|) | f, \mathbf{R}_a; g, \mathbf{R}_b \rangle \\ &\quad + \sum_{\mathbf{r}_a, \mathbf{r}_b} \langle g, \mathbf{R}_a; f, \mathbf{R}_b | U(|\mathbf{r}_a - \mathbf{r}_b|) | g, \mathbf{R}_b; f, \mathbf{R}_a \rangle \end{aligned} \quad (11)$$

where

$$U(|\mathbf{r}_a - \mathbf{r}_b|) = \frac{e^2}{\epsilon |\mathbf{r}_a - \mathbf{r}_b|},$$

and \mathbf{r}_a and \mathbf{r}_b are position vectors of the charge carriers with origins at the center of the quantum dots at \mathbf{R}_a and \mathbf{R}_b respectively. The background dielectric constant, $\epsilon = \epsilon_0 \epsilon_r$ where the relative permittivity, ϵ_r is assumed to be independent of the location of charge carriers. In the two-particle interaction matrix element

$$\langle g, \mathbf{R}_a; f, \mathbf{R}_b | U(|\mathbf{r}_a - \mathbf{r}_b|) | f, \mathbf{R}_a; g, \mathbf{R}_b \rangle,$$

the states to the right of the scattering potential $U(|\mathbf{r}_a - \mathbf{r}_b|)$ represent the initial states while those to the left represent the final scattered states. The first matrix term in Eq. 11 is due to Coulomb interaction in which the excited electron in its initial state f in the quantum dot at \mathbf{R}_a and a hole in the g th state in the quantum dot at \mathbf{R}_b get scattered through the potential U to final states in which the electron and hole remain in the same excited states but their positions are exchanged. The net effect can be viewed as a tunnelling process in which the exciton gets physically transferred from one quantum dot to another. The second matrix element in Eq. 11 represents the scattering of an electron in its initial state f in the quantum dot at \mathbf{R}_a and a hole in the g th state in the quantum dot at \mathbf{R}_b through the potential U such that they remain on their respective quantum dot sites but their excited states are exchanged. This second process can be viewed as one in which the excited electron in one quantum dot recombines with the hole in the ground state and the liberated energy is transferred to excite the electron-hole pair in a neighbouring quantum dot. We assume that the quantum dots are separated by a distance, $W = |\mathbf{R}_a - \mathbf{R}_b|$ such that $W \gg |\mathbf{r}_a - \mathbf{r}_b|$ so that tunneling effects are negligible. The interdot Förster energy transfer process is then determined by the second matrix element in Eq. 11.

Substituting expressions for $|\mathbf{R}_a\rangle$ and $|\mathbf{R}_b\rangle$ (see Eq. 1) into Eq. 11 and employing the Förster multipole expansion of the Coulomb interaction we obtain:

$$\begin{aligned} \langle \mathbf{R} | \hat{H}_F | \mathbf{L} \rangle &= \frac{\nu_0^2}{4\pi\epsilon |\mathbf{R}_a - \mathbf{R}_b|^3} \sum_{\mathbf{r}_e, \mathbf{r}_h} \sum_{\mathbf{r}'_e, \mathbf{r}'_h} \Psi(\mathbf{R}_a, \mathbf{r}_{e\parallel}, \mathbf{r}_{h\parallel}) \Psi^*(\mathbf{R}_b, \mathbf{r}'_{e\parallel}, \mathbf{r}'_{h\parallel}) \\ &\quad \times \varphi_e(z_e) \varphi_h(z_h) \varphi_e^*(z'_e) \varphi_h^*(z'_h) \delta_{\mathbf{r}_e, \mathbf{r}_h} \delta_{\mathbf{r}'_e, \mathbf{r}'_h} \\ &\quad \times [\mu_a \cdot \mu_b - 3(\mu_a \cdot \mathbf{R}_d)(\mu_b \cdot \mathbf{R}_d)] \end{aligned} \quad (12)$$

where

$$\mathbf{R}_d = \frac{(\mathbf{R}_a - \mathbf{R}_b)}{|\mathbf{R}_a - \mathbf{R}_b|},$$

and

$$\mu_{\mathbf{a}(\mathbf{b})} = \int u_c(\mathbf{r}) (\mathbf{r}_{\mathbf{a}(\mathbf{b})} - \mathbf{r}) u_v(\mathbf{r}) d\mathbf{r}$$

where $u_c(\mathbf{r})$ and $u_v(\mathbf{r})$ are the respective periodic components of the bulk Bloch functions of the electron and hole. We assume that the Bloch functions are identical in both the quantum dot and barrier materials.

Using Eqs. 3 - 5 in Eq. 12, we obtain:

$$\begin{aligned} F(W) &= \langle \mathbf{R} | \hat{H}_F | \mathbf{L} \rangle \\ &= \sqrt{\frac{11}{8}} \frac{\mu^2}{\epsilon W^3} \left(\frac{2l_e l_h}{l_e^2 + l_h^2} \right) \left(\frac{2l_{ze} l_{zh}}{l_{ze}^2 + l_{zh}^2} \right)^{1/2} \end{aligned} \quad (13)$$

where $\mu = \mu_a \simeq \mu_b$ and $W = |\mathbf{R}_a - \mathbf{R}_b|$. From Eq. 8 one obtains

$$\begin{aligned} \langle \chi_s | \hat{H}_F | \chi_s \rangle &= -\langle \chi_{as} | \hat{H}_F | \chi_{as} \rangle = \sin \beta F(W) \\ \langle \chi_{as} | \hat{H}_F | \chi_s \rangle &= -\cos \beta F(W) \end{aligned} \quad (14)$$

In view of the fact that F is key to the entanglement and the formation of entangled states, $|\chi_s\rangle$ and $|\chi_{as}\rangle$, we expect the inevitable loss of energy to lattice vibrations coupled with the excitation transfer to lead to decoherence and subsequent degradation of qubit states. We will examine this important process in greater detail in the next section.

IV. EXCITONIC QUBIT-PHONON INTERACTION

We consider the exciton state at each quantum dot to be coupled to a continuum of acoustic phonons via both deformation potential and piezoelectric coupling. The acoustic phonons are modelled as bulk modes which is a valid approximation for quantum dots fabricated in barrier materials with almost similar lattice properties such as (In,Ga)As quantum dots with a (Ga,Al)As barrier. The total Hamiltonian of a system of Förster coupled quantum dot interacting with phonons is given by

$$\begin{aligned} \hat{H}_{\text{qb}}^{\text{env}} &= \hat{H}_{\text{ex-qb}} + \hat{H}^{\text{ph}} + \hat{H}_{\text{ex-qb}}^{\text{DP}} \\ &\quad + \hat{H}_{\text{ex-qb},\lambda}^{\text{Piez}} + \hat{H}_F + \hat{H}_F^{\text{ph}} \end{aligned} \quad (15)$$

where $\hat{H}_{\text{ex-qb}}$ is given by Eq. 7 and the matrix elements of \hat{H}_F is defined by the Förster amplitude term F in Eq. 13. \hat{H}^{ph} is the phonon reservoir

$$\hat{H}_{\text{ph}} = \sum_{\mathbf{q}} \hbar \omega_{\mathbf{q}\lambda} b_{\lambda}^{\dagger}(\mathbf{q}) b_{\lambda}(\mathbf{q}),$$

where $b_{\lambda}^{\dagger}(\mathbf{q})$ and $b_{\lambda}(\mathbf{q})$ are the respective creation and annihilation operator of a λ -mode phonon with wave vector \mathbf{q} . The λ -mode is denoted LA for longitudinal acoustic phonons and TA for transverse acoustic phonons. The acoustic phonon energy spectrum is determined by the dispersion relation $\omega_{\mathbf{q}\text{LA}} = v_{\text{LA}} |\mathbf{q}|$ for the longitudinal mode and $\omega_{\mathbf{q}\text{TA}} = v_{\text{TA}} |\mathbf{q}|$ for the transverse mode, with v_{LA} and v_{TA} denoting the corresponding sound velocities.

$\hat{H}_{\text{ex-qb}}^{\text{DP}}$ is the Hamiltonian for excitonic qubit-phonon interaction via deformation potential coupling and is linear in terms of phonon creation and annihilation operators

$$\begin{aligned} \hat{H}_{\text{ex-qb}}^{\text{DP}} &= \sum_{\lambda, \mathbf{q}} \sqrt{\frac{\hbar |\mathbf{q}|^2}{2\rho V \omega_{\mathbf{q}\lambda}}} [M_r \sigma_x + M_p \sigma_z] \\ &\quad \times \left(b_{\lambda}^{\dagger}(-\mathbf{q}) + b_{\lambda}(\mathbf{q}) \right) |n_{\mathbf{q}\lambda}\rangle \langle n_{\mathbf{q}\lambda}| \end{aligned} \quad (16)$$

where $|n_{\mathbf{q}\lambda}\rangle$ denotes the occupation number of λ -mode phonon with wave vector, \mathbf{q} . V is the crystal volume and ρ is the mass density of the material system. D_c and D_v are the respective deformation potential constants for the conduction and valence bands. The terms M_r and M_p are written as

$$M_r = \langle \chi_{as}; n_{\mathbf{q}\lambda} \pm 1 | (D_c e^{i\mathbf{q}\cdot\mathbf{r}_e} - D_v e^{i\mathbf{q}\cdot\mathbf{r}_h}) | \chi_s; n_{\mathbf{q}\lambda} \rangle, \quad (17)$$

and

$$\begin{aligned} M_p &= \langle \chi_s; n_{\mathbf{q}\lambda} \pm 1 | (D_c e^{i\mathbf{q}\cdot\mathbf{r}_e} - D_v e^{i\mathbf{q}\cdot\mathbf{r}_h}) | \chi_s; n_{\mathbf{q}\lambda} \rangle \\ &\quad - \langle \chi_{as}; n_{\mathbf{q}\lambda} \pm 1 | (D_c e^{i\mathbf{q}\cdot\mathbf{r}_e} - D_v e^{i\mathbf{q}\cdot\mathbf{r}_h}) | \chi_{as}; n_{\mathbf{q}\lambda} \rangle \end{aligned} \quad (18)$$

The M_r term describes a decoherence process in which the qubit state $|\chi_s\rangle$ relaxes to the qubit state $|\chi_{as}\rangle$ due to mediation by phonons. The M_p term describes a second type of decoherence process in which a shift occurs in the energy difference between the two qubit states resulting in pure dephasing of the entangled system.

A similar expression as in Eq. 16 can be obtained for the Hamiltonian $\hat{H}_{\text{ex-qb},\lambda}^{\text{Piez}}$ describing exciton-phonon interaction via piezoelectric coupling

$$\begin{aligned} \hat{H}_{\text{ex-qb},\lambda}^{\text{Piez}} &= \sum_{\lambda,\mathbf{q}} \frac{8\pi\epsilon\epsilon_{14}}{\epsilon_0\epsilon_r|\mathbf{q}|^2} \sqrt{\frac{\hbar}{2\rho V\omega_{\mathbf{q}\lambda}}} (\xi_{x,\lambda}q_yq_z + \xi_{y,\lambda}q_xq_z + \xi_{z,\lambda}q_xq_y) \\ &\quad \times [N_r\sigma_x + N_p\sigma_z] (b_\lambda^\dagger(-\mathbf{q}) + b_\lambda(\mathbf{q})) |n_{\mathbf{q}\lambda}\rangle \langle n_{\mathbf{q}\lambda}| \end{aligned} \quad (19)$$

where the relative permittivity, ϵ_r is assumed to be unaffected by the contribution from strain fields associated with acoustic phonon modes. ϵ_{14} is the piezoelectric constant and $\xi_{i,\lambda}$ is the unit vector of polarization of the λ -phonon along the i -direction. Excitonic interactions with phonons due to piezoelectric coupling are highly anisotropic in nature³⁹ and the form of $\hat{H}_{\text{ex-qb},\lambda}^{\text{Piez}}$ depends on the choice of polarization components and the modes associated with λ . Further details of the dependency on LA, TA1 and TA2 modes are given in the next section. N_r and N_p are analogous to M_r and M_p given in Eqs. 17 and 18 respectively

$$N_r = \langle \chi_{as}; n_{\mathbf{q}\lambda} \pm 1 | (e^{i\mathbf{q}\cdot\mathbf{r}_e} - e^{i\mathbf{q}\cdot\mathbf{r}_h}) | \chi_s; n_{\mathbf{q}\lambda} \rangle, \quad (20)$$

and

$$\begin{aligned} N_p &= \langle \chi_s; n_{\mathbf{q}\lambda} \pm 1 | (e^{i\mathbf{q}\cdot\mathbf{r}_e} - e^{i\mathbf{q}\cdot\mathbf{r}_h}) | \chi_s; n_{\mathbf{q}\lambda} \rangle \\ &\quad - \langle \chi_{as}; n_{\mathbf{q}\lambda} \pm 1 | (e^{i\mathbf{q}\cdot\mathbf{r}_e} - e^{i\mathbf{q}\cdot\mathbf{r}_h}) | \chi_{as}; n_{\mathbf{q}\lambda} \rangle \end{aligned} \quad (21)$$

Unlike the M_r and M_p terms, both N_r and N_p vanish as $\mathbf{q} \rightarrow 0$ due to exact cancellation of electron and hole form factors as the piezoelectric coupling constant remains the same for electrons and holes.

We consider the Hamiltonian \hat{H}_F^{ph} in Eq. 15 to be associated with a interdot Förster energy transfer process that proceeds via a one-phonon assisted transfer of excitonic qubits. A one-phonon-assisted decoherence of qubit states is more likely at lower temperatures while multiphonon phonon processes are expected to dominate at higher temperatures. We express \hat{H}_F^{ph} as arising from second-order process involving two Hamiltonians

$$\hat{H}_F^{\text{ph}} = \hat{H}_{\text{ex-qb}}^X \oplus H_F \quad (22)$$

where $X = \text{DP(Piez)}$ for coupling via deformation potential (piezoelectric fields). The relaxation of qubit states occurs via several routes

$$|\chi_s; n_{\mathbf{q}\lambda}\rangle \xrightarrow{\hat{H}_{\text{ex-qb}}^X} |\chi_{as}; n_{\mathbf{q}\lambda} \pm 1\rangle \xrightarrow{\hat{H}_F} |\chi_{as}; n_{\mathbf{q}\lambda} \pm 1\rangle, \quad (23)$$

$$|\chi_s; n_{\mathbf{q}\lambda}\rangle \xrightarrow{\hat{H}_{\text{ex-qb}}^X} |\chi_s; n_{\mathbf{q}\lambda} \pm 1\rangle \xrightarrow{\hat{H}_F} |\chi_{as}; n_{\mathbf{q}\lambda} \pm 1\rangle,$$

$$|\chi_s; n_{\mathbf{q}\lambda}\rangle \xrightarrow{\hat{H}_F} |\chi_s; n_{\mathbf{q}\lambda}\rangle \xrightarrow{\hat{H}_{\text{ex-qb}}^X} |\chi_{as}; n_{\mathbf{q}\lambda} \pm 1\rangle, \quad (24)$$

$$|\chi_s; n_{\mathbf{q}\lambda}\rangle \xrightarrow{\hat{H}_F} |\chi_{as}; n_{\mathbf{q}\lambda}\rangle \xrightarrow{\hat{H}_{\text{ex-qb}}^X} |\chi_{as}; n_{\mathbf{q}\lambda} \pm 1\rangle$$

Likewise, pure dephasing of excitonic qubit state $|\chi_s; n_{\mathbf{q}}\rangle$ can occur via

$$\begin{aligned}
|\chi_s; n_{\mathbf{q}} \lambda\rangle & \xrightarrow{\hat{H}_{\text{ex-qb}}^{\text{X}}} |\chi_{\text{as}}; n_{\mathbf{q}} \lambda \pm 1\rangle \xrightarrow{\hat{H}_{\text{F}}} |\chi_s; n_{\mathbf{q}} \lambda \pm 1\rangle, \\
|\chi_s; n_{\mathbf{q}} \lambda\rangle & \xrightarrow{\hat{H}_{\text{ex-qb}}^{\text{X}}} |\chi_s; n_{\mathbf{q}} \lambda \pm 1\rangle \xrightarrow{\hat{H}_{\text{F}}} |\chi_s; n_{\mathbf{q}} \lambda \pm 1\rangle, \\
|\chi_s; n_{\mathbf{q}} \lambda\rangle & \xrightarrow{\hat{H}_{\text{F}}} |\chi_s; n_{\mathbf{q}} \lambda\rangle \xrightarrow{\hat{H}_{\text{ex-qb}}^{\text{X}}} |\chi_s; n_{\mathbf{q}} \lambda \pm 1\rangle, \\
|\chi_s; n_{\mathbf{q}} \lambda\rangle & \xrightarrow{\hat{H}_{\text{F}}} |\chi_{\text{as}}; n_{\mathbf{q}} \lambda\rangle \xrightarrow{\hat{H}_{\text{ex-qb}}^{\text{X}}} |\chi_s; n_{\mathbf{q}} \lambda \pm 1\rangle
\end{aligned} \tag{25}$$

Pure dephasing of the qubit state $|\chi_{\text{as}}; n_{\mathbf{q}}\rangle$ occurs similarly as shown above for the $|\chi_s; n_{\mathbf{q}}\rangle$ state.

V. EVALUATION OF MATRIX ELEMENTS

Using Eqs. 1, 3, 4 and 5 in Eq. 16, we obtain explicit forms for the following matrix elements

$$\langle \mathbf{L}; n_{\mathbf{q}} \lambda \pm 1 | \hat{H}_{\text{ex-qb}}^{\text{DP}} | \mathbf{L}; n_{\mathbf{q}} \lambda \rangle = \Sigma_D(q_{\parallel}, q_z) e^{-i\mathbf{q} \cdot \mathbf{R}_a} \tag{26}$$

$$\langle \mathbf{L}; n_{\mathbf{q}} \lambda \pm 1 | \hat{H}_{\text{ex-qb}}^{\text{DP}} | \mathbf{R}; n_{\mathbf{q}} \lambda \rangle = \Sigma_D(q_{\parallel}, q_z) e^{-i\mathbf{q} \cdot \frac{(\mathbf{R}_a + \mathbf{R}_b)}{2}} e^{-\frac{W^2}{4L_R^2}} \tag{27}$$

where L_R is defined below Eq. 3 and a similar expression as in Eq. 26 can be obtained for $\langle \mathbf{R}; n_{\mathbf{q}} \lambda \pm 1 | \hat{H}_{\text{ex-qb}}^{\text{DP}} | \mathbf{R}; n_{\mathbf{q}} \lambda \rangle$. The function $\Sigma_D(q_{\parallel}, q_z)$ which is given by

$$\Xi_D(q_{\parallel}, q_z) = \sqrt{\frac{\hbar |\mathbf{q}|^2}{2\rho V \omega_{\mathbf{q}} \lambda}} e^{-\frac{1}{4}L_R^2 q_{\parallel}^2} \left[D_c e^{-\frac{1}{4}l_{ze}^2 q_z^2} e^{-\frac{1}{4}l_e^2 q_{\parallel}^2} - D_v e^{-\frac{1}{4}l_{zh}^2 q_z^2} e^{-\frac{1}{4}l_h^2 q_{\parallel}^2} \right]$$

differs from the commonly used form²⁰ as we consider the non-isotropic propagation of phonon here. From Eqs. 8, 26 and 27 we obtain

$$\begin{aligned}
\langle \chi_{\text{as}}; n_{\mathbf{q}} \lambda \pm 1 | \hat{H}_{\text{ex-qb}}^{\text{DP}} | \chi_s; n_{\mathbf{q}} \lambda \rangle & = \frac{1}{2} \sin(\beta/2) (e^{-i\mathbf{q} \cdot \mathbf{R}_a} - e^{-i\mathbf{q} \cdot \mathbf{R}_b}) \Sigma_D(q_{\parallel}, q_z) \\
& - \cos(\beta/2) e^{-\frac{W^2}{4L_R^2}} \Sigma_D(q_{\parallel}, q_z)
\end{aligned} \tag{28}$$

The first term in Eq. 28 contains the coherence factor $(e^{-i\mathbf{q} \cdot \mathbf{R}_a} - e^{-i\mathbf{q} \cdot \mathbf{R}_b})$ which remains effective over large distances between the quantum dots. The second term involves the factor $e^{-\frac{W^2}{4L_R^2}}$ which is short-ranged as it depends on the overlap integral of the exciton wavefunctions in quantum dots located at different sites. By integrating the coherence factor over the polar angle ϕ , we obtain

$$|\langle \chi_{\text{as}}; n_{\mathbf{q}} \lambda \pm 1 | \hat{H}_{\text{ex-qb}}^{\text{DP}} | \chi_s; n_{\mathbf{q}} \lambda \rangle|^2 = 2\pi \Sigma_D^2(q_{\parallel}, q_z) \left[\frac{1}{2} \sin^2(\beta)(1 - J_0(q_{\parallel}W)) + \cos^2(\beta) e^{-\frac{W^2}{2L_R^2}} \right] \tag{29}$$

where $J_0(q_{\parallel}W)$ is the zeroth-order Bessel function. In order to obtain a tractable form of Eq. 29 we approximate $J_0(q \sin(\theta)W)$ by taking the angular average

$$\begin{aligned}
J_0(q \sin(\theta)W) & \approx \frac{\int \int J_0(q \sin(\theta)W) \sin(\theta) d\theta d\phi}{\int \int \sin(\theta) d\theta d\phi} \\
& = \frac{\sin(qW)}{qW}
\end{aligned}$$

For large separations between the quantum dots, we approximate

$$|\langle \chi_{\text{as}}; n_{\mathbf{q}} \lambda \pm 1 | \hat{H}_{\text{ex-qb}}^{\text{DP}} | \chi_s; n_{\mathbf{q}} \lambda \rangle|^2 \approx \pi \Sigma_D^2(q_{\parallel}, q_z) \sin^2(\beta) \left(1 - \frac{\sin(qW)}{qW}\right)$$

Similar expressions as in Eq. 29 but with slight variations in the dependency on polar angle β can be obtained for $|\langle \chi_{\text{as}}; n_{\mathbf{q}} \lambda \pm 1 | \hat{H}_{\text{ex-qb}}^{\text{DP}} | \chi_{\text{as}}; n_{\mathbf{q}} \lambda \rangle|^2$ and $|\langle \chi_s; n_{\mathbf{q}} \lambda \pm 1 | \hat{H}_{\text{ex-qb}}^{\text{DP}} | \chi_s; n_{\mathbf{q}} \lambda \rangle|^2$. These expressions will be used in Eqs. 17

and 18 to evaluate the rates at which the excitonic qubits lose their decoherence via relaxation and dephasing in the following section.

In the case of qubit-phonon interaction via piezoelectric coupling, we use a choice of phonon polarization components with respect to the cubic crystallographic axes of the zinc-blende type crystal. Substituting Eqs. 1, 3, 4 and 5 into Eq. 19, we get explicit forms for the following matrix elements

$$\langle \mathbf{L}; n_{\mathbf{q}\lambda} \pm 1 | \hat{H}_{\text{ex-qb},\lambda}^{\text{Piez}} | \mathbf{L}; n_{\mathbf{q}\lambda} \rangle = \Sigma_P(q_{\parallel}, q_z, \lambda) e^{-\mathbf{q}_{\parallel} \cdot \mathbf{R}_a} \quad (30)$$

$$\langle \mathbf{L}; n_{\mathbf{q}\lambda} \pm 1 | \hat{H}_{\text{ex-qb},\lambda}^{\text{Piez}} | \mathbf{R}; n_{\mathbf{q}\lambda} \rangle = \Sigma_P(q_{\parallel}, q_z, \lambda) e^{-\mathbf{q}_{\parallel} \cdot \frac{(\mathbf{R}_a + \mathbf{R}_b)}{2}} e^{-\frac{w^2}{4L_R^2}} \quad (31)$$

where the function $\Sigma_P(q_{\parallel}, q_z, \lambda)$ is defined as

$$\Sigma_P(q_{\parallel}, q_z, \lambda) = \frac{4\pi e e_{14}}{\epsilon_0 \epsilon_r} \sqrt{\frac{\hbar}{2\rho V v_{\lambda} q}} A_{\lambda}(\theta, \phi) e^{-\frac{1}{4}L_R^2 q_{\parallel}^2} \left[e^{-\frac{1}{4}l_{ze}^2 q_z^2} e^{-\frac{1}{4}l_{le}^2 q_{\parallel}^2} - e^{-\frac{1}{4}l_{zh}^2 q_z^2} e^{-\frac{1}{4}l_{lh}^2 q_{\parallel}^2} \right] \quad (32)$$

The anisotropy factor $A_{\lambda}(\theta, \phi)$ is given by

$$A_{\text{LA}}(\theta, \phi) = \frac{3}{4} \sin 2\theta \sin \theta \sin 2\phi, \quad (33)$$

$$A_{\text{TA1}}(\theta, \phi) = \frac{1}{8} (\sin \theta - \sin 3\theta) \sin 2\phi, \quad (34)$$

$$A_{\text{TA2}}(\theta, \phi) = \frac{1}{2} \sin 2\theta \cos 2\phi \quad (35)$$

The TA1 and TA2 modes correspond to the two possible polarized direction of the transverse phonon. Calculations of the square amplitude term $|\langle \chi_{\text{as}}; n_{\mathbf{q}\lambda} \pm 1 | \hat{H}_{\text{ex-qb},\lambda}^{\text{Piez}} | \chi_s; n_{\mathbf{q}\lambda} \rangle|^2$ where $\lambda = \text{LA}, \text{TA1}, \text{TA2}$ are slightly involved due to the presence of the polar angle ϕ in Eq. 33 - 35. For $\lambda = \text{LA}$, we obtain

$$|\langle \chi_{\text{as}}; n_{\mathbf{q}\text{LA}\pm 1} | \hat{H}_{\text{ex-qb,LA}}^{\text{Piez}} | \chi_s; n_{\mathbf{q}\text{LA}} \rangle|^2 = \frac{\pi}{4} \Sigma_P^2(q_{\parallel}, q_z, \text{LA}) \left[\sin^2(\beta) \left(1 - \frac{\sin(qW)}{qW}\right) + 9 \cos^2(\beta) e^{-\frac{w^2}{2L_R^2}} \right] \quad (36)$$

where $\Sigma_P(q_{\parallel}, q_z, \text{LA})$ can be obtain using Eqs. 32 and 33. Similar expressions as in Eq. 36 can be obtained for the TA1 and TA2 modes of the transverse phonon using Eqs. 34 and 35.

VI. DECOHERENCE RATES OF EXCITONIC QUBITS

The decoherence rates associated with relaxation and pure dephasing processes are calculated using

$$\frac{1}{\tau_{X,\lambda}} = \frac{2\pi}{\hbar} \sum_{q_{\parallel}, q_z} |\langle f | \hat{H}_{\text{int}} | i \rangle|^2 (N_{\mathbf{q},\lambda} + 1) \delta(\Delta E \pm \hbar\omega_{\mathbf{q}\lambda}) \quad (37)$$

where $|i\rangle$ and $|f\rangle$ denote the initial and final states which are functions of $|\chi_{\text{as}}\rangle$ and $|\chi_s\rangle$ (see Eqs. 17, 18, 20 and 21). ΔE is the energy difference between the initial and final states which determines the wavevector of the emitted phonon. H_{int} is the interaction operator which is substituted by $\hat{H}_{\text{ex-qb}}^{\text{DP}}$ or $\hat{H}_{\text{ex-qb},\lambda}^{\text{Piez}}$ depending on the type of phonon coupling. In the case of decoherence associated with Förster transfer process, H_{int} is given by $\hat{H}_{\text{F}}^{\text{ph}}$ as will be detailed in the next section. $N_{\mathbf{q}\lambda}$ is the thermalised average number of phonons at the temperature T , and is given by the Bose-Einstein distribution $N_{\mathbf{q}\lambda} = \exp(\hbar\omega_{\mathbf{q}\lambda}/k_B T)$ where k_B is the Boltzmann constant.

From Eqs. 17, 18, 29 and 37 we obtain explicit expressions for the rate of relaxation ($1/\tau_{\text{DP}}^r$) and rate of dephasing ($1/\tau_{\text{DP}}^p$) of excitonic qubits

$$1/\tau_{\text{DP}}^{r(p)} = \frac{(D_c - D_v)^2 q^3}{4\sqrt{\pi}\hbar\rho v_{\text{LA}}^2} \exp\left(-\frac{3}{4}q^2 l^2\right) \frac{\text{Erfi}(\Delta l)}{\Delta l} (N_{\mathbf{q},\lambda} + 1) S_{r(p)}(\beta) \quad (38)$$

where the functions $S_r(\beta)$ and $S_p(\beta)$ are given by

$$S_r(\beta) = \frac{1}{2} \sin^2(\beta) \left(1 - \frac{\sin(qW)}{qW}\right) + \cos^2(\beta) e^{-\frac{w^2}{l^2}} \quad (39)$$

$$S_p(\beta) = \frac{1}{2} \cos^2(\beta) \left(1 - \frac{\sin(qW)}{qW}\right) + \frac{1}{2} \sin^2(\beta) e^{-\frac{w^2}{l^2}}$$

To simplify the derivation of Eq. 38, we have used the assumptions that $l_e \approx l_h = l$ and $l_{ze} \approx l_{zh} = l_z$. $\text{Erfi}(\Delta l)$ is the imaginary error function, $\Delta l = q\sqrt{\frac{1}{2}(\frac{3}{2}l^2 - l_z^2)}$ and $q = \frac{2F(W)}{\hbar v_{\text{LA}}}\sqrt{1 + \gamma^2}$ where $\gamma = \frac{\Delta\Omega}{2F(W)}$ (see Eq. 13 for an analytical expression for $F(W)$). It can be noted that the cut-off frequency in Eq. 38 occurs at $\omega_l \sim v_{\text{LA}}/l$ which is approximately the inverse phonon flight time through the quantum dot.

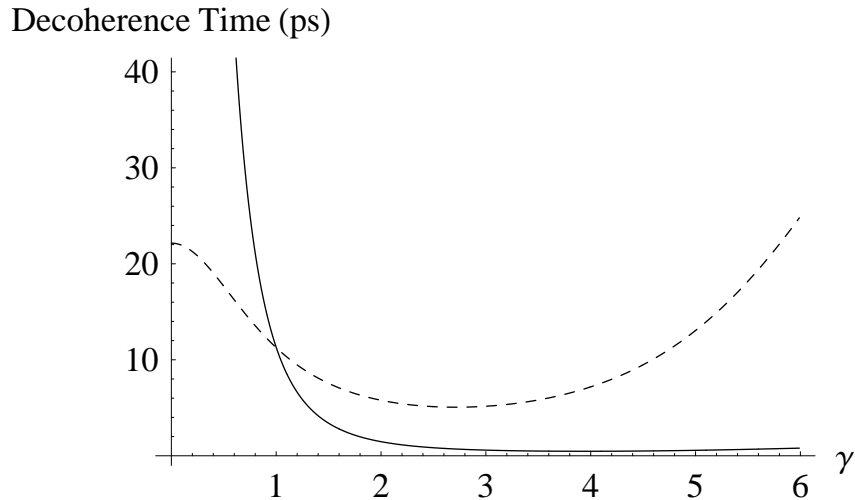


FIG. 1: Relaxation time τ_{DP}^r (dashed) and dephasing time, τ_{DP}^p (full) as functions of $\gamma = \frac{\Delta\Omega}{2F(W)}$ at $T = 10$ K, $W = 5$ nm, $l_e \approx l_h = l = 2.5$ nm and $l_{ze} \approx l_{zh} = l_z = 2.5$ nm.

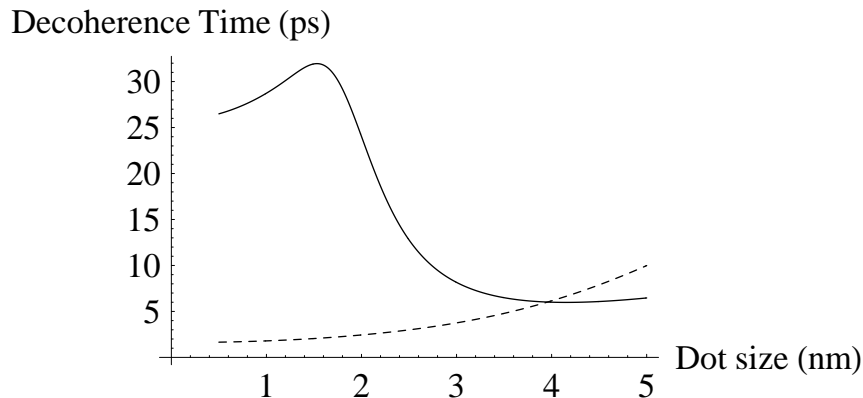


FIG. 2: Relaxation time, τ_{DP}^r (dashed) and dephasing time τ_{DP}^p (full) as functions of dot size l at $\gamma = 0.25$, $W = 4$ nm, $l_z = 1$ nm and $T = 10$ K.

Using the parameters for the GaAs/AlGaAs material system³⁹, we calculate the relaxation time τ_{DP}^r and dephasing time τ_{DP}^p as functions of γ in Fig. 1. At $\gamma = 0$, the qubit states are maximally entangled and decoherence is dominated by the relaxation process as one can expect from two equally populated states. As γ increases, the difference in the population of the qubit states is enhanced and decoherence becomes increasingly dominated by pure dephasing process. We note that the minimum in relaxation time τ_m^r is reached at γ_m and is given by $\tau_m^r \approx W/2\pi v_{\text{LA}}$ thus satisfying the condition where the interdot separation matches the phonon wavevector. At small values of γ , the quantum dot size parameter l has a stronger influence on the dephasing process as shown in Fig. 2 where the dephasing time decreases sharply after $l \approx 2$ nm while the relaxation time increases gradually mainly determined by the exponential term in Eq. 38. Fig. 3 shows that at critical values of W (depending on γ and l), the relaxation times can reach very small

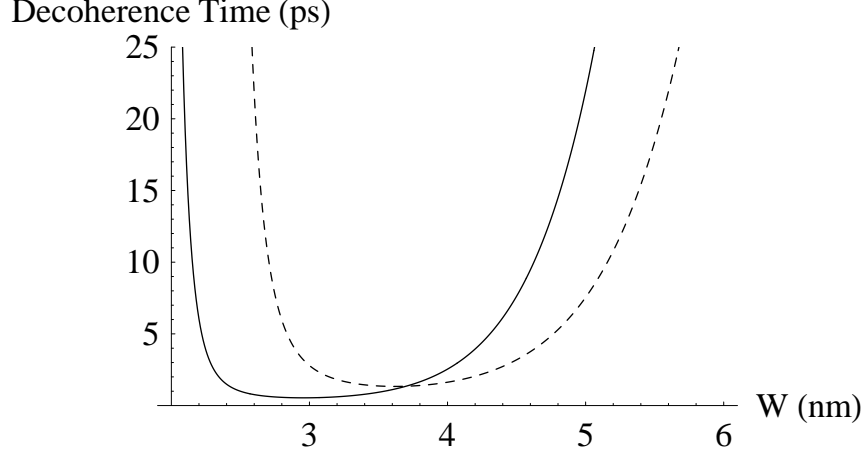


FIG. 3: Relaxation time τ_{DP}^r as function of interdot distance W at $\gamma = 1.5$ (dashed) and $\gamma = 0.1$ (full) at $l = 2$ nm, $l_z = 1$ nm and $T = 10$ K.

values in the order of several picoseconds.

In the case of qubit-phonon interaction via piezoelectric coupling, we obtain the relaxation and dephasing rates for $\lambda = \text{LA}$, using Eqs. 17, 18, 36 and 37

$$1/\tau_{\text{Piez}}^{r(p)} = \frac{\pi^2 q e^2 e_{14}^2}{2\epsilon^2 \hbar \rho v_{\text{LA}}^2} \exp(-q^2 l^2 / 2) \left[1 - \exp\left(-\frac{1}{4}(r^2 - 1)q^2 l^2\right) \right]^2 G_{\text{LA}}\left(\frac{q^2 l^2 r^2}{2(r^2 + 1)}\right) (N_{\mathbf{q}, \lambda} + 1) S'_{r(p)}(\beta) \quad (40)$$

where $r = l_h/l_e$ and we have used the assumption that $l = l_e = l_{ze}$ in order to obtain an analytical expression. The function $G_{\text{LA}}(x)$ is given by

$$G_{\text{LA}}(x) = \frac{2x + 15}{4x^3} - \frac{\sqrt{\pi} e^{-x} (4x(x + 3) + 15) \text{Erfi}(\sqrt{x})}{8x^{7/2}} \quad (41)$$

and $S'_r(\beta)$ and $S'_p(\beta)$ are given by

$$\begin{aligned} S'_r(\beta) &= \sin^2(\beta) \left(1 - \frac{\sin(qW)}{qW}\right) + 9 \cos^2(\beta) e^{-\frac{w^2}{l^2}} \\ S'_p(\beta) &= \cos^2(\beta) \left(1 - \frac{\sin(qW)}{qW}\right) + \frac{9}{2} \sin^2(\beta) e^{-\frac{w^2}{l^2}} \end{aligned} \quad (42)$$

Similar expressions as in Eq. 40 but with terms $G_{\text{TA1}}(x)$ and $G_{\text{TA2}}(x)$ associated with TA1 and TA2 modes are obtained for qubits interacting with transverse acoustic phonons

$$\begin{aligned} G_{\text{TA1}}(x) &= \frac{3}{2x^2} - \frac{\sqrt{\pi} e^{-x} (2x + 3) \text{Erfi}(\sqrt{x})}{4x^{5/2}} \\ G_{\text{TA2}}(x) &= \frac{\sqrt{\pi} e^{-x} (x(x(2x + 5) + 12) + 15) \text{Erfi}(\sqrt{x})}{6x^{7/2}} - \frac{x(x + 2) + 15}{3x^3} \end{aligned} \quad (43)$$

As expected $1/\tau_{\text{Piez}}^{r(p)} = 0$ when $l_h = l_e$ due to piezoelectric coupling being a polar mechanism.

Fig 4 shows that dephasing process due to qubits interacting with phonons via deformation potential is the dominant mechanism of decoherence for larger values of γ (≥ 2.5) while the relaxation process dominates at small values of γ . As expected, these features are similar to those obtained in the case of phonon coupling via deformation potential. These results as well as those obtained for the deformation potential case highlight the critical role of γ and quantum dot parameters in influencing the decoherence properties of excitonic qubit systems. Therefore the quality factor Q^{14} which determines the number of charge oscillations that can be resolved within the decoherence time can be selected using the quantum dot system configuration based on parameters l , l_z , r , W and T . It appears that phonon assisted decoherence can be suppressed by careful choice of system parameters leading to higher fidelity of logic gate operation. In the next section we consider another source of decoherence involving one-phonon assisted Förster transfer process.

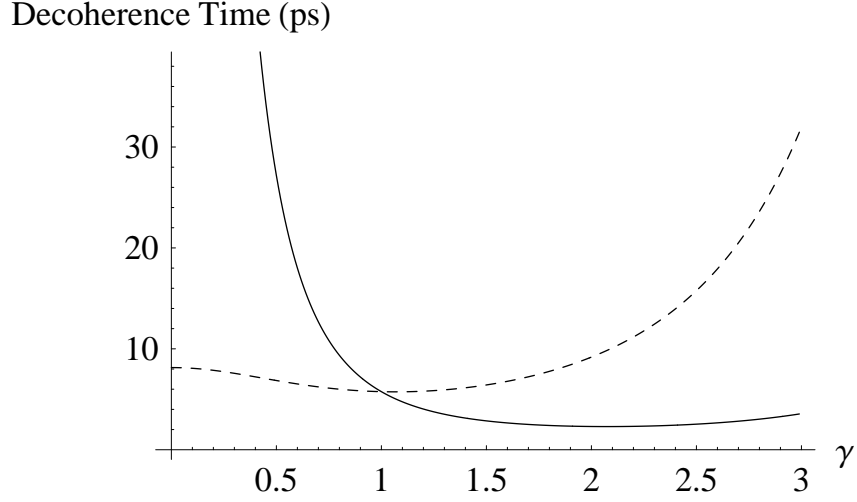


FIG. 4: Relaxation time, τ_{Piez}^r (dashed) and dephasing time τ_{Piez}^p (full) as functions of γ at $W = 5$ nm, $l_e = l_{ze} = 2$ nm, $r = l_h/l_e = 5$ and $T = 10$ K.

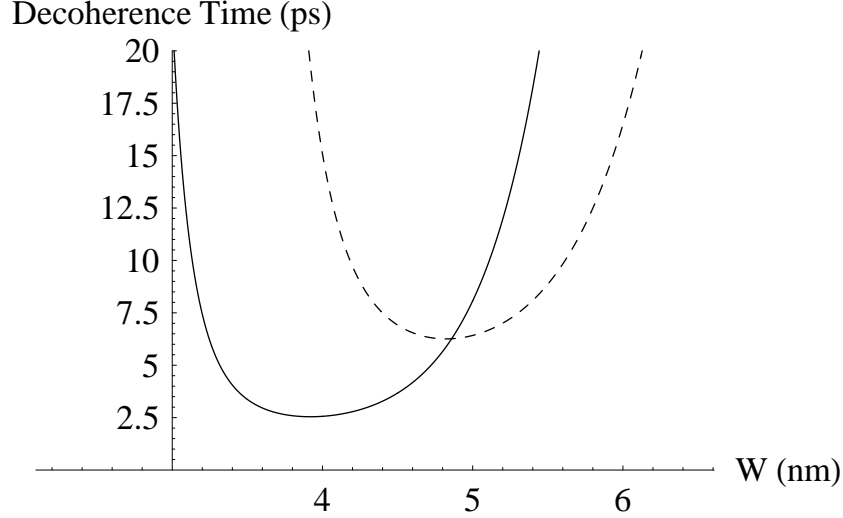


FIG. 5: Relaxation time τ_{Piez}^r as function of interdot distance W at $\gamma = 1.5$ (dashed) and $\gamma = 0.1$ (full) at $l_e = l_{ze} = 2$ nm, $r = 5$ and $T = 10$ K.

VII. DECOHERENCE ASSOCIATED WITH ONE-PHONON ASSISTED FÖRSTER TRANSFER PROCESS

The decoherence rate, $\frac{1}{T_{X,\lambda}}$ associated with phonon assisted Förster relaxation process is obtained using Eq. 37 where \hat{H}_{int} is evaluated via

$$|\langle f | \hat{H}_{\text{F}}^{\text{ph}} | i \rangle|^2 = \frac{1}{4} \left| \sum_{i=1}^4 T_{r,x}^i \right|^2 \quad (44)$$

where $X = \text{DP}$ or Piez and $T_{r,X}^i$ are the transition amplitudes associated with qubit relaxation. $T_{r,X}^1$ and $T_{r,X}^2$ for example are obtained using Eqs. 23 and 24

$$T_{r,X}^1 = \mp \frac{1}{\hbar\omega_{\mathbf{q}\lambda}} \langle \chi_{\text{as}}; n_{\mathbf{q}\lambda} \pm 1 | \hat{H}_F | \chi_{\text{as}}; n_{\mathbf{q}\lambda} \pm 1 \rangle \langle \chi_{\text{as}}; n_{\mathbf{q}\lambda} \pm 1 | \hat{H}_{\text{ex-qb}}^X | \chi_s; n_{\mathbf{q}\lambda} \rangle \quad (45)$$

$$T_{r,X}^4 = \pm \frac{1}{\hbar\omega_{\mathbf{q}\lambda}} \langle \chi_{\text{as}}; n_{\mathbf{q}\lambda} \pm 1 | \hat{H}_{\text{ex-qb}}^X | \chi_s; n_{\mathbf{q}\lambda} \rangle \langle \chi_s; n_{\mathbf{q}\lambda} | \hat{H}_F | \chi_s; n_{\mathbf{q}\lambda} \rangle \quad (46)$$

In the case of dephasing mechanism, we use

$$|\langle f | \hat{H}_F^{\text{ph}} | i \rangle|^2 = \frac{1}{8} \left[\left| \sum_{i=1}^4 |T_{p,s}^i|^2 - \left| \sum_{i=1}^4 |T_{p,\text{as}}^i|^2 \right| \right] \quad (47)$$

where the transition amplitudes $T_{p,s}^i$ are evaluated using Eqs. 25 - 25. The transition amplitudes $T_{p,\text{as}}^i$ associated with transitions between the χ_{as} is obtained analogous to Eq. 44.

By neglecting the interference between terms in Eqs. 44, we obtain explicit terms for the rates of relaxation and dephasing

$$1/\tau_{\text{DP,F}}^{r(p)} = \frac{(D_c - D_v)^2 q^3}{32\sqrt{\pi}\hbar(1 + \gamma^2)\rho v_{\text{LA}}^2} \exp(-\frac{3}{4}q^2 l^2) \frac{\text{Erfi}(\Delta l)}{\Delta l} (N_{\mathbf{q},\lambda} + 1) S_r^F(\beta) \quad (48)$$

$$(49)$$

where $\gamma = \frac{\Delta\Omega}{2F(W)}$ and the functions $S_r^F(\beta)$ and $S_p^F(\beta)$ are given by

$$S_r^F(\beta) = \sin^4(\beta) + \frac{1}{2} \cos^2(\beta)(3 + \cos 2\beta) + \sin(2\beta)e^{-\frac{W^2}{l^2}} + \left[\frac{1}{4} \sin^2(2\beta) - \sin^4(\beta) \right] \frac{\sin(qW)}{qW} \quad (50)$$

$$S_p^F(\beta) = 8 \sin^3(\beta) \frac{\sin(qW/2)}{qW} e^{-\frac{W^2}{2l^2}}$$

The combined rates of relaxation and dephasing for qubits coupled to the LA, TA1 and TA2 modes of the acoustic phonons associated with the piezoelectric fields are obtained as

$$1/\tau_{\text{Piez,F}}^{r(p)} = \frac{\pi^{3/2} q e^2 e_{14}^2}{16\epsilon^2 (1 + \gamma^2) \hbar \rho v_{\text{LA}}^2} \exp(-q^2 l^2 / 2) \left[1 - \exp\left(-\frac{(r^2 - 1)q^2 l^2}{4}\right) \right]^2 G_{\text{LA}}\left(\frac{q^2 l^2 r^2}{2(r^2 + 1)}\right) (N_{\mathbf{q},\lambda} + 1) S_r^{F'}(\beta) \quad (51)$$

where the function $G_r(x)$ is obtained using Eq. 41 and associated functions, $G_{\text{TA1}}(x)$ and $G_{\text{TA2}}(x)$ (see Eq. 43) and the functions $S_r^{F'}(\beta)$ and $S_p^{F'}(\beta)$ are given by

$$S_r^{F'}(\beta) = g_1(\beta) + g_2(\beta)e^{-\frac{W^2}{l^2}} + g_3(\beta) \frac{\sin(qW)}{qW} \quad (52)$$

$$S_p^{F'}(\beta) = g_4(\beta) \frac{\sin(qW/2)}{qW} e^{-\frac{W^2}{2l^2}}$$

where $g_i(x), i = 1, \dots, 4$ can be obtained using Eqs. 33, 34 and 35.

Fig. 6 shows that pure dephasing dominates at low values of γ in a one-phonon assisted Förster transfer process while the relaxation process is the preferred mode of decoherence at higher values of γ . These features are in reverse of those obtained in Fig. 1 where the phonon mediated process takes place in the vicinity of individual quantum dots. At very small values of γ , the decoherence times reach values of the order of several picoseconds showing the significant loss of coherence which occurs during charge carrier oscillations between qubit states. Fig. 7 shows that relaxation via phonon-assisted Förster transfer process is a more likely route for decoherence than the direct mode of relaxation at large interdot separations and small γ values. The notable oscillations in relaxation times is possibly due to matching of the interdot separation with multiples of the phonon wavevector as γ is increased. In Fig. 8 we note the reverse effects on the two types of decoherence mechanisms due to an increase in size parameter l

Fig. 9 shows that the one-phonon assisted Förster transfer process associated with piezoelectric fields proceeds in the same manner as in the model involving deformation potential. Fig. 10 highlights the range of W for which decoherence times can match typical logic gate times of around 10 - 50 ps. In the presence of an external electric field, energy for both electrons and holes is reduced with larger dots experiencing bigger shifts. We expect changes to the order of at most a magnitude to the results obtained here.

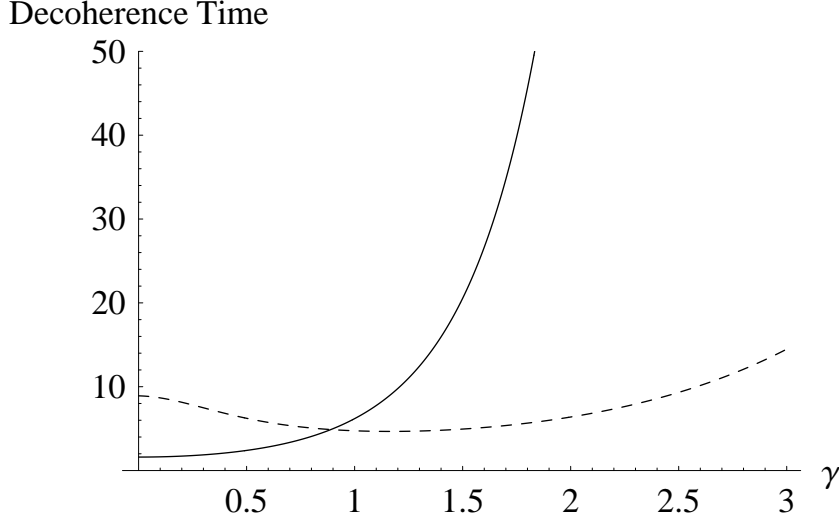


FIG. 6: Comparison of relaxation time $\tau_{\text{DP,F}}^r$ (dashed) and dephasing time $\tau_{\text{DP,F}}^p$ (full) due to deformation potential coupling as function of γ at $W = 4$ nm (full), $l = 2$ nm, $l_z = 1$ nm and $T = 10$ K.

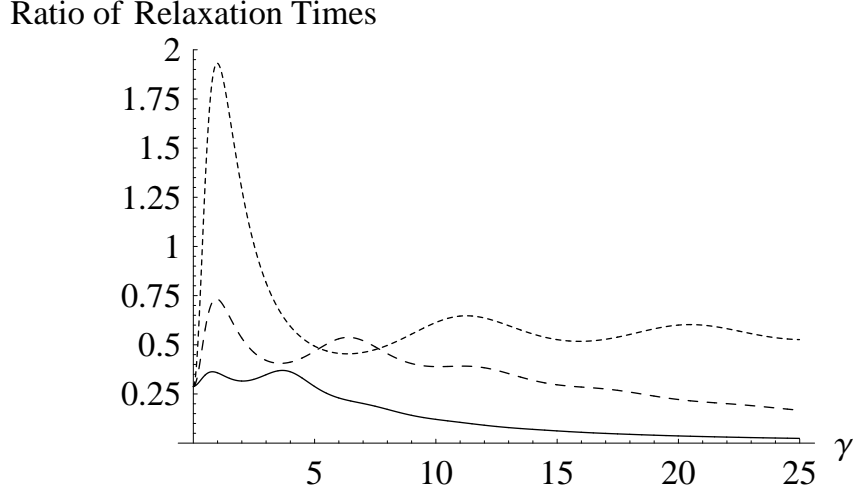


FIG. 7: Ratio of relaxation times $\frac{\tau_{\text{DP,F}}^r}{\tau_{\text{DP,F}}^p}$ as function of γ at $W = 4$ nm (full), 5 nm (dashed), 6.5 nm (dotted) and 1 = 2 nm, $l_z = 1$ nm and $T = 10$ K.

VIII. BERRY PHASE AND CONCURRENCE OF THE COMPOSITE EXCITON SYSTEM

We evaluate two important quantities, namely the Berry phase and concurrence of the composite exciton system in quantum dots. We consider a simplified model in which the Förster interaction is switched off after $t=0$ and assume that there is no correlation between the phonon bath interacting with the correlated electron-hole pairs at different quantum dots. The Hamiltonian in Eq. 15 can be solved³⁷ to produce an explicit expression for the reduced density matrix of the two qubits system at a later time t . The overall initial density matrix ($\rho_T(0)$) of the system of qubits and phonon reservoir, $\rho_{ph}(0)$ is obtained as

$$\rho_T(0) = \rho_{ex}(0)^L \otimes \rho_{ex}(0)^R \otimes \rho_{ph}^L(0) \otimes \rho_{ph}^R(0). \quad (53)$$

where $\rho_{ex}(0)^L$ and $\rho_{ex}(0)^R$ are the initial density matrix states of the two-state qubit system (see Eq. 6). $\rho_{ph}^L(0)$ and $\rho_{ph}^R(0)$ are density matrices associated with the phonon reservoir in the quantum dots at $|\mathbf{R}_a\rangle$ and $|\mathbf{R}_b\rangle$, respectively.

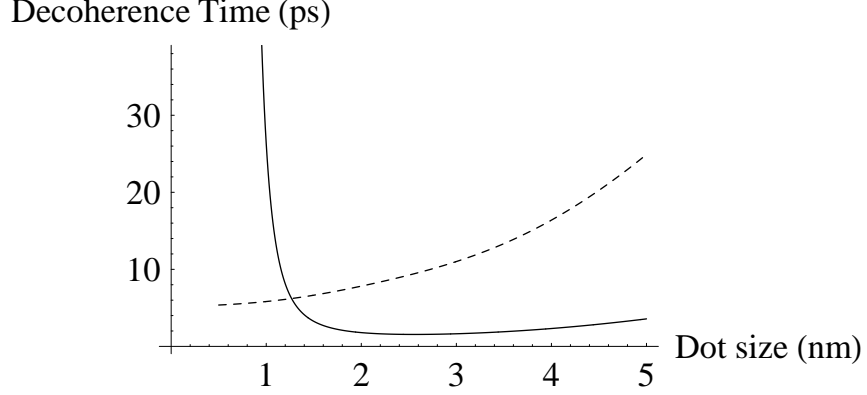


FIG. 8: Relaxation time, $\tau_{DP,F}^r$ (dashed) and dephasing time $\tau_{DP,F}^p$ (full) as functions of dot size l at $\gamma = 0.25$, $W = 4$ nm, $l_z = 1$ nm and $T = 10$ K.

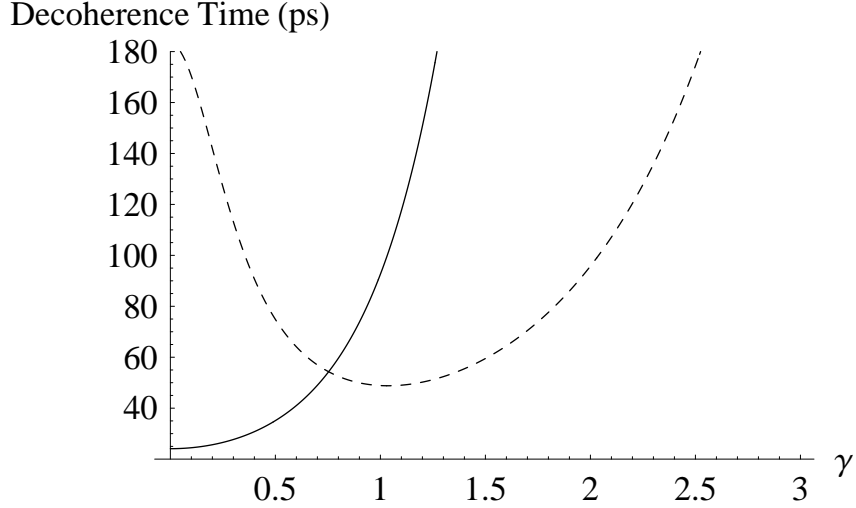


FIG. 9: Comparison of relaxation time $\tau_{Piez,F}^r$ (dashed) and dephasing time $\tau_{Piez,F}^p$ (full) due to piezoelectric field as function of γ at $W = 5$ nm (full), $l = 2$ nm, $r = 5$ nm and $T = 10$ K.

At $t = 0$, each phonon reservoir is assumed to be thermalized at temperature T

$$\rho_{ph}^I(0) = \prod_{\mathbf{q}} (1 - e^{-\frac{\omega_{\mathbf{q}}}{k_B T}}) e^{-\frac{\omega_{\mathbf{q}}}{k_B T} b_{\mathbf{q}}^\dagger b_{\mathbf{q}}} . \quad (54)$$

where $I = L, R$.

We consider an initial state given by $|\chi_s\rangle = \cos(\beta(0)/2) |\mathbf{L}\rangle + \sin(\beta(0)/2) |\mathbf{R}\rangle$ (see Eq. 8) which depends on the interdot Förster interaction amplitude F at $t = 0$ through the angle $\beta(0)$. We will show later that the evolution of β with time is dependent on the dynamics of interaction between the qubit states and phonon bath. In the case of identical qubits, the state $\rho_T(t) = |\chi_s\rangle \langle \chi_s|$ evolves according to

$$\rho_T(t) = \begin{pmatrix} 0 & 0 & 0 & 0 \\ 0 & \cos^2(\beta/2) & \frac{1}{2} \sin(\beta(0)) e^{i\Delta\Omega t} Z(t) & 0 \\ 0 & \frac{1}{2} \sin(\beta(0)) e^{-i\Delta\Omega t} Z(t) & \sin^2(\frac{\beta(0)}{2}) & 0 \\ 0 & 0 & 0 & 0 \end{pmatrix} . \quad (55)$$

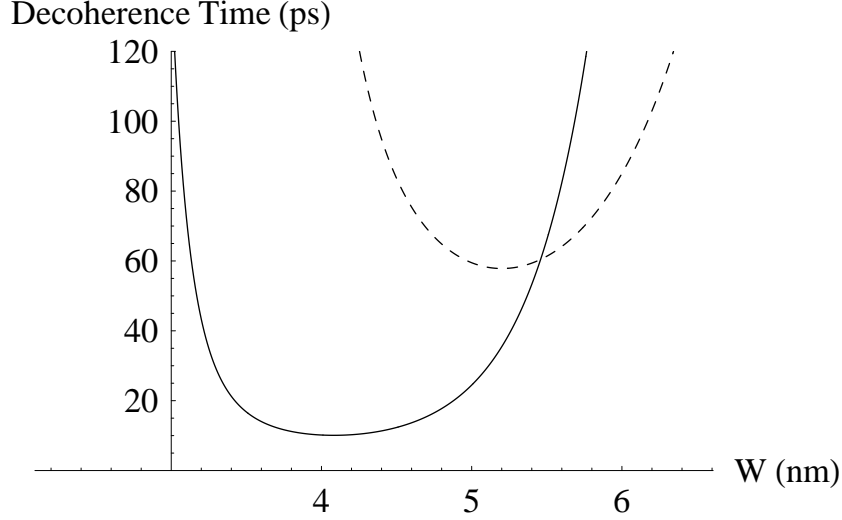


FIG. 10: Relaxation time $\tau_{\text{Piez,F}}^r$ as function of interdot distance W at $\gamma = 1.5$ (dashed) and $\gamma = 0.1$ (full) at $l = 2$ nm, $r = 5$ nm and $T = 10$ K.

where $\Delta\Omega$ is the difference in exciton creation energy between the two quantum dots and $Z(t) = e^{-4[G_L(t)+G_R(t)]}$ provides a measure of the decay of the off-diagonal matrix elements when each qubit is isolated from the other, but exposed to its own reservoir of phonon bath. The function $G(t) = \exp(-2 \int \frac{d\omega}{\hbar\omega^2} J(\omega) \coth(\hbar\omega/2k_B T) \sin^2(\omega t/2))$ where $J(\omega)$ is the spectral density function which yields information about the interaction of the quantum dot with the phonons⁴⁰

$$J_D(\omega) = \sum_{\mathbf{q}} \Xi_D(q_{\parallel}, q_z)^2 \delta(\omega - \omega_{\mathbf{q}}) \quad \text{Deformation Potential} \quad (56)$$

$$J_P(\omega, \lambda) = \sum_{\mathbf{q}} \Sigma_P(q_{\parallel}, q_z, \lambda)^2 \delta(\omega - \omega_{\mathbf{q}}) \quad \text{Piezoelectric Interaction} \quad (57)$$

where $\Xi_D(q_{\parallel}, q_z)$ and $\Sigma_P(q_{\parallel}, q_z, \text{LA})$ are given in Eqs. 28 and 32 respectively. At small ω , $J(\omega) \sim \omega^k$ where the exponent k determines between the cases of ohmic ($k = 1$), sub- ($k < 1$) and superohmic ($k > 1$) couplings⁴¹. The explicit expressions for $J_D(\omega)$ and $J_P(\omega, \text{LA})$ are determined using Eqs. 29 and 36 to be in superohmic forms where $k = 3$ and $k = 5$ respectively for $J_D(\omega)$ and $J_P(\omega, \text{LA})$.

The Berry phase of a mixed state is defined as

$$\eta = \arg \left[\sum_j \sqrt{E_j(0)E_j(T)} \langle \chi_j(0) | \chi_j(T) \rangle e^{-\int_0^T dt \langle \chi_j(t) | \dot{\chi}_j(t) \rangle} \right] \quad (58)$$

where the system frequency $\Delta\Omega$ determines the quasi-cyclic path of the geometric phase with time t varying from 0 to $T = \frac{2\pi}{\Delta\Omega}$. $E_j(T)$ and $\chi_j(T)$ refer to the eigenvalues and eigenvectors, respectively of the density matrix in Eq. 55

$$\begin{aligned} E_{\pm}(t) &= \frac{1}{2} \pm \frac{1}{2} (\cos^2(\beta) + \exp(-2G(t)) \sin^2(\beta))^2 \\ |\chi_+(t)\rangle &= \cos\left(\frac{\beta(t)}{2}\right) |\mathbf{R}\rangle + \sin\left(\frac{\beta(t)}{2}\right) |\mathbf{L}\rangle \end{aligned} \quad (59)$$

where $\tan(\frac{\beta(t)}{2}) = \exp(-G(t)) \cot(\frac{\beta(0)}{2})$, and the evolution of the phase is determined only by $|\chi_+(t)\rangle$ as $E_-(0) = 0$. At $t = 0$, $G(t) = 0$, $Z(t) = 1$ and $|\chi_+(t)\rangle \rightarrow |\chi_s(0)\rangle$. Substituting Eq. 59 into Eq. 58 we evaluate $\eta = \eta_0 + \eta_c$ where $\eta_0 = \pi(1 - \cos(\beta))$ is the well known result for a unitary evolution at $G(t) = 0$. The unitary phase correction term η_c which appears when $G(t) \neq 0$ is evaluated using series expansion of $G(t)$.

Fig. 11 shows the increase of Berry phase correction fraction $\frac{\eta_c}{\eta}$ with temperature in GaAs/AlGaAs quantum dots coupled to phonon baths via deformation potential. The geometric phase of the qubit state undergoes a greater degree of nonunitary evolution within a superohmic environment at larger temperatures. At $T = 0$ K, zero point

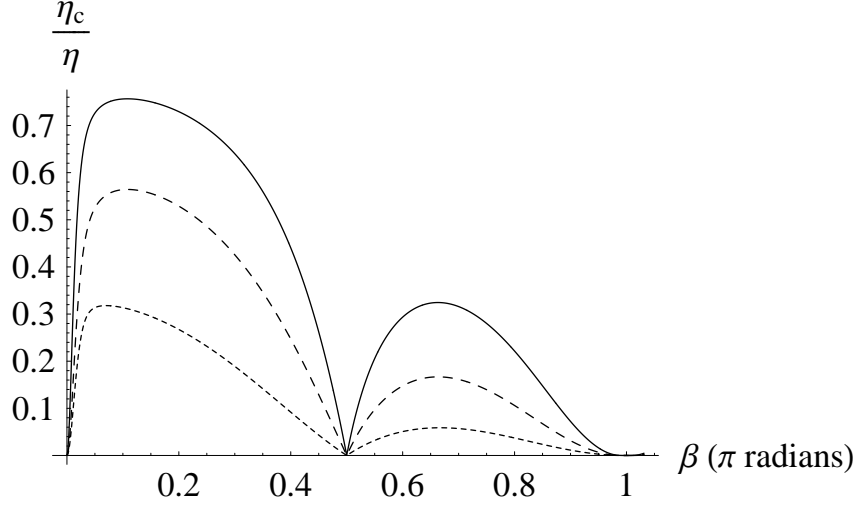


FIG. 11: Berry phase correction fraction $\frac{\eta_c}{\eta}$ as function of polar angle β due to decoherence associated with deformation potential at $W = 5$ nm, $l = 1$ nm and $T = 120$ K (full), 50 K (dashed) and $T = 0$ K (dotted)

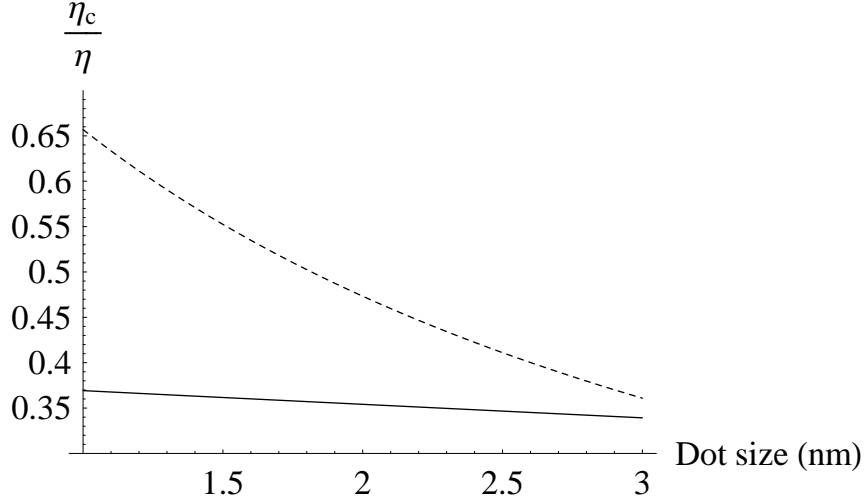


FIG. 12: Berry phase correction fraction $\frac{\eta_c}{\eta}$ as function of the dot size due to decoherence associated with deformation potential (dashed) and piezoelectric coupling (full) at $W = 5$ nm, $\beta = \frac{\pi}{4}$ and $T = 100$ K.

fluctuations associated with a noisy environment contributes to the non-zero correction in Berry phase. At $\beta = n\pi$ where n is an integer, $T = \frac{2\pi}{\Delta\Omega}$ vanishes so that the system stagnates and $\frac{\eta_c}{\eta} = 0$ at the nodal points. At $\beta = n\frac{\pi}{2}$, T becomes very large and that the system never completes its quasi-cyclic path and there is negligible phase correction. At other values of β , the departure from unitary behavior is clearly dependent on the spectral density function $G(t)$ as the Bloch sphere is altered according to $G(t)$. There is decreased effect of decoherence effects on η as the phase angle sweeps the second quarter to complete the first half of cyclic evolution.

Fig. 12 shows the gradual decrease of Berry phase correction and hence progress towards a more unitary evolution at larger quantum dot sizes for both types of phonon couplings. The difference between the two curves can be attributed to microscopic properties of the spectral density functions $J_D(\omega)$ and $J_P(\omega)$. In both cases, the density function rises rapidly with ω and reach peak values at an optimum ω_m before starting to decrease at even higher values of ω . Fig. 13 shows the increase of Berry phase correction with interdot distance W which gives a measure of the degree of entanglement at $t = 0$. It is to be noted that W provides a direct link between concurrence (details below) and correction to the Berry phase. At large W , the concurrence of the qubit states at $t = 0$ is weak and the Berry phase is less immune to decoherence effects and undergoes a higher degree of non-unitary evolution at $t \geq 0$.

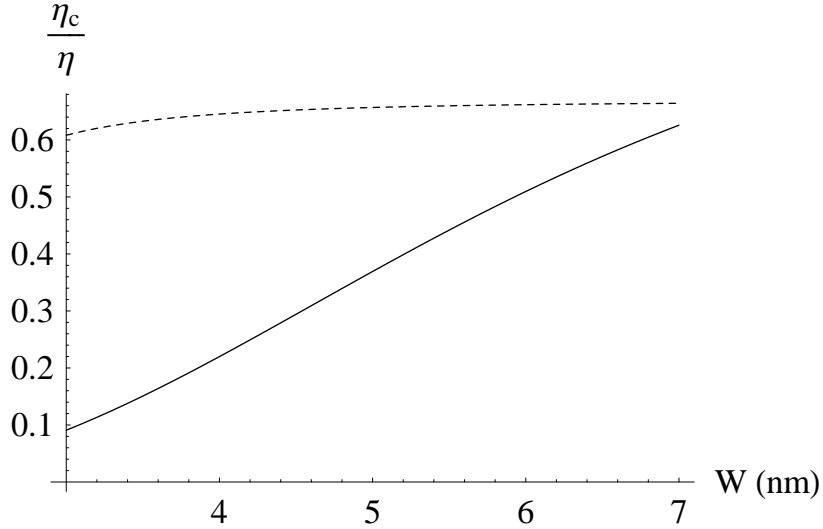


FIG. 13: Berry phase correction fraction $\frac{\eta_c}{\eta}$ as function of interdot distance W due to decoherence associated with deformation potential (full) and piezoelectric coupling (dashed) at $W = 5$ nm, $\beta = \frac{\pi}{4}$ and $T = 100$ K.

The evolution of the entanglement between the subsystems $\rho_{ex}(0)^L$ and $\rho_{ex}(0)^R$ is determined by a quantity termed concurrence, $C(t)$ which is related to the entanglement of formation³⁸. For a pure or mixed state, ρ_T , of two qubits, the spin-flipped state is defined as

$$\tilde{\rho}_T = (\sigma_y \otimes \sigma_y) \rho_T^* (\sigma_y \otimes \sigma_y), \quad (60)$$

where σ_y belongs to the set of Pauli matrices. The concurrence is given by³⁸

$$C(\rho_T(t)) = \max \left\{ 0, 2 \max_i \lambda_i - \sum_{j=1}^4 \lambda_j \right\}. \quad (61)$$

where λ_i s are the square roots of the eigenvalues of the non-Hermitian matrix $\rho_T \tilde{\rho}_T$ with each value of λ_i being a non-negative real number.

The eigenvalues of the matrix product $\rho_T \tilde{\rho}_T$ for the density matrix Eq. 55 are

$$\lambda_{1,2} = \frac{1}{2} \sin(\beta) (Z(t) \pm 1), \quad (62)$$

and $\lambda_{3,4} = 0$. Hence the concurrence is obtained as

$$C(t) = \frac{1}{2} \sin(\beta) e^{-4[G_L(t)+G_R(t)]} \quad (63)$$

Figs. 14 and 15 show differences in half times of concurrence decay in GaAs/AlGaAs quantum dots which are isolated from each other but each exposed to their own phonon baths via deformation potential and piezoelectric coupling. The half time during which half of the initial entanglement at $t = 0$ is lost is less for qubits interacting with phonons via deformation potential compared the qubit-phonon system incorporating piezoelectric coupling. These differences can be attributed to functions $G_D(t)$ and $G_P(t)$. The function $G_D(t)$ associated with the spectral density functions $J_D(\omega)$ (deformation potential) rises with time and reaches a constant value whereas $G_P(t)$ retains its monotonic increase with time. Both figures show an increase of half time with quantum dot size l which is due to the shorter time needed for the phonons to travel the length of the quantum dot and decrease of spectral density function $J(\omega)$ as the dot size is increased. It is to be noted that in our model we have considered lattice vibrations at the two qubit locations to be uncorrelated so that the bath modes are independent unlike the model incorporating a common environment used by Braun³⁴.

IX. CONCLUSIONS

We have studied several processes that contribute to the decoherence of excitonic qubits in quantum dot systems coupled by the Förster-type transfer process. We show the significant loss of coherence that occurs through charge

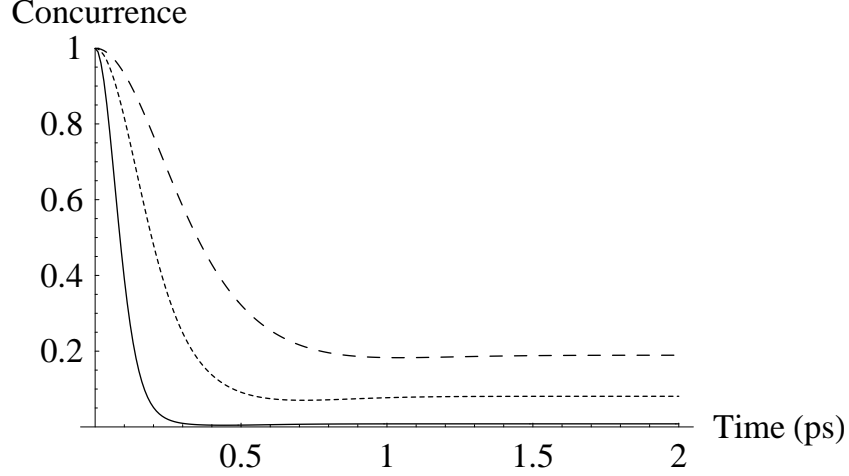


FIG. 14: Concurrence decay in qubits coupled to uncorrelated phonon baths via deformation potential coupling at $l = 2$ nm (dashed), 1 nm (full), 1.5 nm (dotted) and $T = 10$ K, with the prefactor $\frac{1}{2} \sin(\beta)$ suppressed.

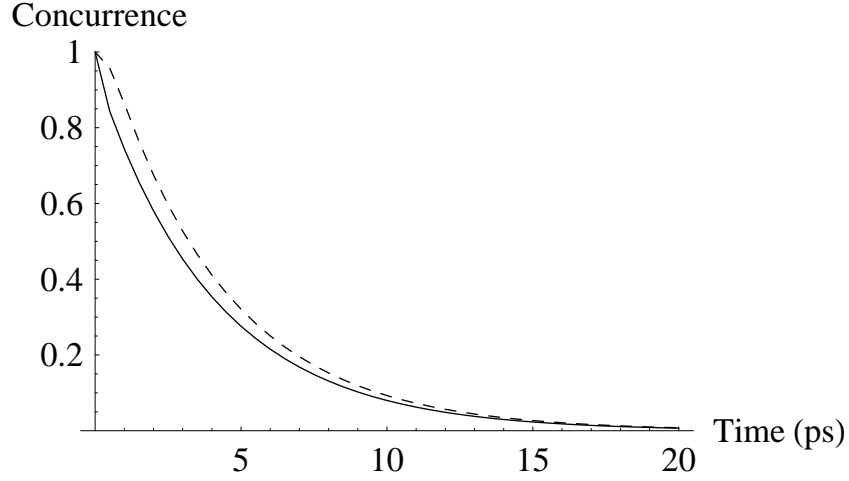


FIG. 15: Concurrence decay in qubits coupled to uncorrelated phonon baths via piezoelectric coupling at $l = 3$ nm (dashed), 0.5 nm (full) and $T = 10$ K, with the prefactor $\frac{1}{2} \sin(\beta)$ suppressed.

carrier oscillations between the different qubit states by using a model of one-phonon assisted Förster-type transfer process. It is shown that increasing a tuning factor γ has opposite effects on the relaxation and dephasing times for excitonic qubits interacting with acoustic phonons via both deformation potential and piezoelectric coupling. Our results show that entanglement of qubits which are isolated from each other last for comparatively long times when interacting with uncorrelated phonons baths via deformation potential compared to the case of piezoelectric coupling which become completely disentangled within 20 ps. The results obtained here show that phonon mediated interactions exert a sizable influence on the non-unitary evolution of Berry phase in quantum dot systems. Lastly, our results emphasise the strong correlation between the Berry phase correction fraction which quantify departure from unitary evolution and half times of concurrence decay in GaAs/AlGaAs quantum dots.

¹ D. Loss and D. P. DiVincenzo, Phys. Rev. A **57**, 120 (1998).

- ² E. Biolatti, R. C. Iotti, P. Zanardi, F. Rossi, Phys. Rev. Lett. **85**, 5647 (2000).
- ³ X. Li, Y. Wu, D. Steel, D. Gammon, T. H. Stievater, D. S. Katzer, D. Park, C. Piermarocchi, L. J. Sham, Science **301**, 809 (2003).
- ⁴ H. J. Krenner, S. Stuffer, M. Sabathil, E. C. Clark, P. Ester, M. Bichler, G. Abstreiter, J. J. Finley, and A. Zrenner, New J. Phys. **7**, 184 (2005).
- ⁵ A. Muller et al., Appl. Phys. Lett. **84**, 981 (2004) L. Besombes, J. J. Baumberg and J. Motohisa, Phys. Rev. Lett. **90**, 257402 (2003)
- ⁶ A. Zrenner et al, Nature **418**, 612 (2002)
- ⁷ Brendon W. Lovett, John H. Reina, Ahsan Nazir and G. Andrew D. Briggs, Phys. Rev. B **68**, 205319 (2003)
- ⁸ Ahsan Nazir, Brendon W. Lovett and G. Andrew D. Briggs, Phys. Rev. A **70**, 52301 (2004)
- ⁹ Ahsan Nazir, Brendon W. Lovett, Sean D. Barrett, John H. Reina and G. Andrew D. Briggs, Phys. Rev. B **71**, 45334(2005)
- ¹⁰ T. Förster, Ann. Phys. (Leipzig) **2**, 55 (1948)
- ¹¹ D. L. Dexter, J. Chem. Phys. **21**, 836 (1953)
- ¹² D. A. Lidar, I. L. Chuang and K. B. Whaley, Phys. Rev. Lett. **81**, 2594 (1998)
- ¹³ P. Zanardi and M. Rasetti, Phys. Rev. Lett. **79**, 3306 (1997)
- ¹⁴ U. Hohnenester, Phys. Rev. B **74**, 161307(R) (2006)
- ¹⁵ P. Xue and Y. P. Xiao, Phys. Rev. Lett. **97**, 140501 (2006)
- ¹⁶ G. Falci, R. Fazio, G. M. Palma, J. Siewet, and V. Vedral, Nature (London) **407**, 355 (2000)
- ¹⁷ P. Solinas, P. Zanardi, N. Zanghi, and F. Rossi, Phys. Rev. B **67**, 121307(R) (2003)
- ¹⁸ S. L. Zhu and P. Zanardi, Phys. Rev. A **72**, 020301(R) (2006)
- ¹⁹ T. Takagahara, Phys. Rev. Lett. **71**, 3577 (1993)
- ²⁰ L. Fedichkin and A. Fedorov, Phys. Rev. A **69**, 032311 (2004)
- ²¹ T. Hayashi, T. Fujisawa, H. D. Cheong, Y. H. Jeong and Y. Hirayama, Phys. Rev. Lett. **91**, 226804 (2003)
- ²² L. Jacak, P. Hawrylak, and A. Wojs, *Quantum Dots* (Springer Verlag, Berlin, 1998)
- ²³ L. Jacak, J. Krasnyj, D. Jacak, and P. Machnikowski, Phys. Rev. B **65**, 113305 (2002)
- ²⁴ P. Machnikowski, Phys. Rev. Lett. **96**, 140405 (2006)
- ²⁵ W. H. Zurek, Rev. Mod. Phys. **75**, 715 (2003)
- ²⁶ T. Unold, K. Mueller, C. Lienau, T. Elsaesser, and A. D. Wieck, Phys. Rev. Lett. **94**, 137404 (2005).
- ²⁷ J. I. Climente, A. Bertoni, G. Goldoni and E. Molinari, Phys. Rev. B **74**, 035313 (2006)
- ²⁸ Z. J. Wu, K. D. Zhu, X. Z. Yuan, Y. W. Jiang and H. Zheng, Phys. Rev. B **71**, 205323 (2005)
- ²⁹ S. Nomura and T. Kobayashi, Solid State Commun. **82**, 335 (1992)
- ³⁰ V. Privman, J. Stat. Phys. **110**, 957 (2003)
- ³¹ I. de Vega, D. Alonso, P. Gaspard and W. T. Strunz, The Journal of Chemical Physics, **122**, 124106 (2005)
- ³² M. Wenin and W. Pötz, Phys. Rev. A **74**, 022319 (2006)
- ³³ M. Esposito and F. Haake (quant-ph/0510164) and M. Esposito, Ph. D. Thesis, cond-mat/0412495
- ³⁴ D. Braun, Phys. Rev. Lett. **89**, 277901 (2002)
- ³⁵ Z. Ficek and R. Tanas, Phys. Rev. A **74**, 24304 (2006)
- ³⁶ T. Yu and J. H. Eberly, Phys. Rev. Lett. **93**, 140404 (2004)
- ³⁷ D. Tolkunov, V. Privman and P. K. Arvind, Phys. Rev. A **71**, 060308(R) (2005)
- ³⁸ W. K. Wootters, Phys. Rev. Lett. **80**, 2245 (1998)
- ³⁹ A. Thilagam and M. A. Lohe, J. Phys. Condens. Matter **18**, 3157 (2006)
- ⁴⁰ A. J. Leggett, S. Chakravarty, A. T. Dorsey, M. P. A Fisher, A. Garg, and W. Zwerger, Rev. Mod. Phys. **59**,1 (1987)
- ⁴¹ B. Krummheuer, V. M. Axt, and T. Kuhn, Phys. Rev. B **65**, 195313 (2002)